CHEMISTRY
A European Journal

A Journal of
ChemPubSoc Europe

Accepted Article

Title: A Multifunctional Pincer Ligand Supports Unsaturated Cobalt: Five Functionalities in One Pincer

Authors: Alexander V Polezhaev, Chun-Hsing Chen, Yaroslav Losovyj, and Kenneth G. Caulton

To be cited as: *Chem. Eur. J.* 10.1002/chem.201700859

Link to VoR: http://dx.doi.org/10.1002/chem.201700859

Supported by
ACES

WILEY-VCH

10.1002/chem.201700859

WILEY-VCH

FULL PAPER

A Multifunctional Pincer Ligand Supports Unsaturated Cobalt: Five Functionalities in One Pincer

Alexander V. Polezhaev, Chun-Hsing Chen, Yaroslav Losovyj and Kenneth G. Caulton*[a]

Abstract: A pyridyl pincer ligand is introduced to incorporate steric bulk, via a P^{t}Bu$_2$ arm, and proton responsivity, via a pyrazole pincer ligand arm, together with reactivity at benzylic hydrogen and redox activity within a 1,4 diazabutadiene moiety. Binding it to $CoCl_2$ yields square pyramidal (PNNH)$CoCl_2$, that is deprotonated with Li[N(SiMe$_3$)$_2$] forming [Li(THF)$_2$PNN]$CoCl_2$. Reduction of this LiCl adduct with KC_8 under CO atmosphere leads to formation of Co(I) mono- and dicarbonyls, which can be protonated but also be further deprotonated, at the benzylic CH, leading to a dearomatized pyridyl functionality. The ligand is characterized in its neutral, monoanionic and dianionic forms, and the anions are shown to be intimate ion pairs with Li^+ bound to pyrazolate N and chloride bound to Lewis acidic cobalt. X-ray photoelectron spectroscopy is used to assay both Li content and cobalt oxidation states. The general character of binding of LiCl to a metal complex acidic at metal and nucleophilic at ligand (pyrazolate-Nβ) is discussed, as are potential catalytic applications of the concept.

Introduction

We are targeting multielectron and multiproton reduction processes for transformation of hard-to-reduce molecules, such as N_2 and CO_2 into valuable chemicals[1]. It was earlier shown by Floriani[2] for CO_2 and recently by Holland[3] for N_2 that alkali metal cations can play an important role in such a process, acting as a templating element in multimetallic reactions. We have been exploring a *bis*-pyrazole pyridine ligand (H_2L) (Fig. 1) and have begun to establish the general characteristics of this diprotic acid as follows: It binds well in the tridentate meridional fashion, and is proton responsive via the protons on the β nitrogens[4]. When deprotonated, the anionic pyrazolate becomes a peripherally directed nucleophile, coordinating to alkali metal cations, but also readily bridging to a second transition metal, leading to aggregation. In the event that the metal in a *bis*-pyrazol*ate* pyridyl complex is unsaturated, then it combines, in close proximity, both Lewis acid and Lewis base character, with the potential reactivity of a single molecule Frustrated Lewis Pair (FLP) (i.e binding both nucleophile and electrophile); this concept has already been recognized for some metal-ligand interactions[5]. The idea behind FLP is that steric bulk prevents direct interaction between Lewis acid and Lewis base but substrate can bind *between* FLP partners. In H_2L-based complexes, Lewis acidic (metal) and Lewis basic (pyrazolyl-β-nitrogen) sites cannot quench intramolecularly, but intermolecular binding occurs rapidly, leading to dimers or polymers. To prevent dimerization, steric bulk must be introduced in the ligand.

There is currently an immense amount of activity on pincer ligands containing two bulky phosphine arms connected by an aryl or pyridyl central donor (Fig. 1), and their modular character allows systematic modification, for various applications[6], including activation of small molecules[7]. We were especially interested in *combining* the features of these *two* pincer ligands by creating a ligand with one bulky phosphine arm and one pyrazolate arm (Fig. 1) in an effort to prevent dimerization.

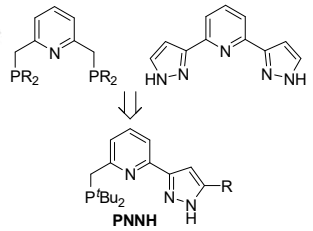

Figure 1. Combining two functionalities in one ligand.

Additional features of phosphorus incorporation can be easily recognized including ^{31}P NMR spectroscopy for reaction monitoring of diamagnetic species, and the two ^{t}Bu groups allow sensing any mirror plane of symmetry containing the pincer plane, a feature absent in the *bis*-pyrazolyl pyridine ligand. We hoped to synthesize metal complexes in varied oxidation states/geometries and the flexibility of the phosphine arm could help to achieve geometries impossible for rigid *bis*-pyrazolyl pyridine. An unusual feature of the PNN^{-1} ligand is that an anionic center is located in the arm, not in a core of the ligand like in majority of monoanionic pincers, positioning it *cis* to incoming substrate.

The PNNH ligand contains *two* acidic protons: one on the β-nitrogen of pyrazole ring and the second one on the benzylic position. These have very different acidity, so could be removed stepwise (Scheme 1a). Removal of pyrazolic protons creates a negative charge on the ligand and also a strong donor site on the β-nitrogen that could carry alkali metal cation or interact with a second transition metal with formation of M_2 or MM' species. The benzylic hydrogens which link the phosphorus to the pyridine ring are particularly reactive and removal of one of these as a proton unmasks anionic charge which is also stabilized at the pyridine

[a] Dr. A. V. Polezhaev, Dr. C.-H. Chen, Dr. Yaroslav Losovyj, Prof. Dr. K. G. Caulton
Department of Chemistry
Indiana University Bloomington
47405, Bloomington, IN (USA)
E-mail: caulton@indiana.edu

Supporting information containing CV, XPS, NMR, IR spectra, and crystallographic information for this article is given via a link at the end of the document

10.1002/chem.201700859

nitrogen (Scheme 1b). In sum, the electronegative nitrogen of pyridine is much more potent for encouraging these *cooperative or bifunctional* behaviors than would be true if that were a phenyl ring[8]. Considering also the P and two types of N lone pair donors, the PNNH ligand thus incorporates an unusually large number of functionalities. Both of these deprotonations are redox neutral at the metal, but have the added benefit of creating additional unsaturation at the metal, via chloride abstraction, as envisioned in Scheme 1a.

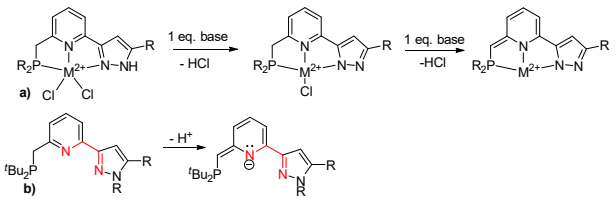

Scheme 1. Proposed stepwise deprotonation of PNNH ligand.

We report here on our initial observations with such a ligand on cobalt in different oxidation states. We thus challenge a three-coordinate Co(I) complex to *additionally* coordinate both nucleophile and electrophile and explore the redox and acid/base chemistry of designed ligand.

Results and Discussion

Synthesis and characterization of Co^{II} Complexes

The ligands with phenyl and *tert*-butyl groups on C5 pyrazole carbon were synthesized to manage solubility; all phenyl derivatives showed lower solubility than their tert-butyl analog. The synthesis was performed in 3 steps with excellent yields using Claisen condensation of 2-methyl-6-methoxycarbonylpyridine with pinacolone or acetophenone followed by hydrazine treatment with formation of pyrazole ring and subsequent treatment of doubly deprotonated heterocycle by $^{t}Bu_2PCl$ (Scheme 2). The structure of products was confirmed by ^{1}H, ^{31}P and ^{13}C NMR.

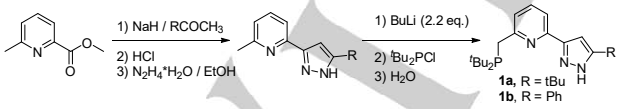

Scheme 2. Synthesis of PNNH ligands.

Reaction of equimolar $CoCl_2$ and $PNN^{tBu}H$ **1a** in THF occurs in 12 h at r.t. After concentration of the reaction mixture and addition of Et_2O, a deep violet precipitate was separated (Scheme 3). Its ^{1}H NMR spectrum in CD_2Cl_2 shows, with correct intensities, signals for all ring proton environments, including that of the NH proton, and 18:9 intensity signals for two types of ^{t}Bu groups. Given the chemical shift range -2 to 74 ppm, the molecule is paramagnetic. Seeing one signal for the two ^{t}Bu groups on phosphorus suggests (incorrectly) a mirror plane relating those two. An ion of m/z 453.1 with characteristic isotope distribution appears in the positive mode of both ESI and APCI mass spectrum, corresponding to $[(PNN^{tBu}H)CoCl]^{+}$. Metallation of $PNN^{Ph}H$ was performed under the same conditions and spectroscopic data (Figure 2) are very similar for both $[PNN^{tBu}H]CoCl_2$ **2a** and $[PNN^{Ph}H]CoCl_2$ **2b**.

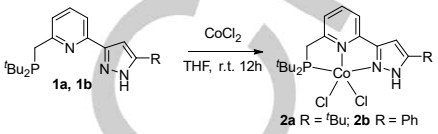

Scheme 3. Metallation of $PNN^{R}H$ **1a** and **1b** with $CoCl_2$.

Single crystal X-ray diffraction of a crystal of $(PNN^{tBu}H)CoCl_2$ **1a** grown by slow diffusion of pentane vapors in concentrated THF solution at -45°C enhances what is learned from spectroscopy. The molecule crystallizes with one lattice guest molecule of THF, whose oxygen hydrogen bonds to the NH proton (Figure 3). The molecule is square pyramidal, τ_5 = 0.3, where a value of 0 is square pyramid and 1 is trigonal bipyramidal[9]. The two chlorides are therefore chemically inequivalent, with one located *trans* to the empty coordination site. The two ^{t}Bu on P are also inequivalent. One phosphine ^{t}Bu group is directed towards that empty site, but the Co/C distance, >3.7 Å, shows no bonding, but simply filling otherwise empty space. Another indication of no agostic interaction is that both Co-P-C(quaternary) angles are similar at ~ 118°. The Co/N distance to pyrazole is shorter than that to pyridine.

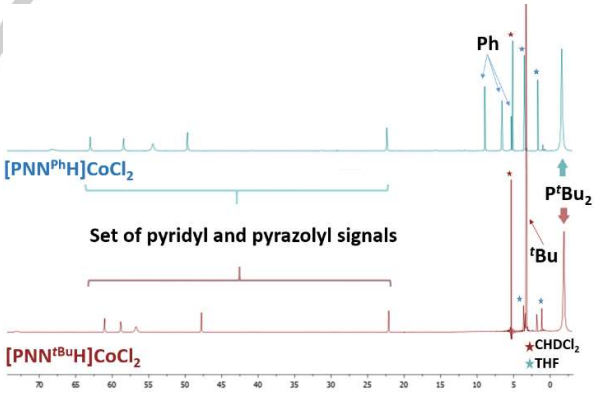

Figure 2. ^{1}H NMR spectra of $(PNN^{tBu}H)CoCl_2$ **2a** and $(PNN^{Ph}H)CoCl_2$ **2b** in CD_2Cl_2.

The ground state structure found shows that the nonrigidity characteric of five coordinate species pertains here: a simple intramolecular rearrangement which puts the axial Cl trans to pyridine nitrogen while the second chlorine moves to an apical position is a low energy process, and dynamically averages the

10.1002/chem.201700859

environments of the two ^{t}Bu groups on phosphorus, giving only one ^{t}Bu ^{1}H NMR chemical shift. Another feature which distinguishes this ligand from its C_2-symmetric variants with either two pyrazolates or two phosphines is its nonplanarity: cobalt does not lie in the plane of the three donor atoms, although it does lie in the plane of the pyridine and pyrazole rings. This is also evident in the nonplanarity of the ring containing phosphorus and also the small angle N3Co1P1, which has a value of only 95°. A THF molecule hydrogen bonds to a pyrazole β-nitrogen proton (3.139 Å N1/O1) typical of moderate hydrogen bonds[10] and also previously observed between THF and other H-pyrazole containing complexes[4, 11].

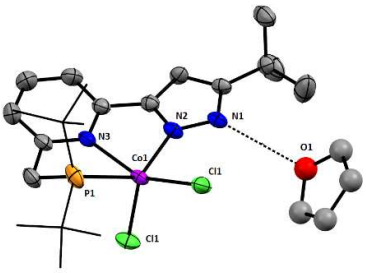

Figure 3. Mercury view (50% probability) of the nonhydrogen atoms of (PNN^{tBu}H)CoCl$_2$ **2a**, showing selected atom labelling; unlabeled atoms are carbon. Selected structural parameters: Co1-Cl1, 2.307; Co1-Cl2, 2.287; Co1-P1, 2.480; Co1-N2, 2.079; Co1-N3, 2.207; Cl1-Co1-Cl2, 111.46; Cl1-Co1-P1, 104.43; Cl2-Co1-P1, 103.57; Cl1-Co1-N2, 91.26; Cl2-Co1-N2, 108.30; Cl1-Co1-N3, 154.61; Cl2-Co1-N3, 92.97. ^{t}Bu groups on phosphorous atom are shown as wireframe, for clarity.

Pyrazole Deprotonation.

Treatment of violet slurry of (PNN^{R}H)CoCl$_2$ **2a** or **2b** with equimolar LiN(SiMe$_3$)$_2$ (LiHMDS) in THF at -78°C results in immediate color change from violet to blue. After warming up to room temperature and removal of the solvent, blue residue was obtained in nearly quantitative yield. The ESI$^+$ mass spectrum of THF solution of the product **3a** shows ions at 905.2 and 911.1 m/z corresponding to dimers of formula ([(PNN^{tBu}H)CoCl]$_2$+H)$^+$, and ([(PNN^{tBu}H)CoCl]$_2$+Li)$^+$, respectively and a small peak at 949.1 m/z corresponding to ([((PNN^{tBu}H)CoCl]$_2$+LiCl+H)$^+$ (all with characteristic isotope patterns due to ^{35}Cl and ^{37}Cl natural abundance) proving that LiCl is a part of the complex. The product is not simply the dehydrohalogenation species (PNN^{tBu})Co^{II}Cl. Dicobalt species in the mass spectrum indicate an unexpected tendency of lithium to aggregate multiple ligand/cobalt moieties.

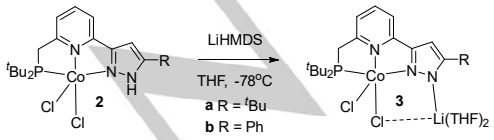

Scheme 4. Deprotonation of (PNN^{R}H)CoCl$_2$ **2a** and **2b**.

The ^{1}H NMR spectrum of **3a** in THF-d_8 shows, with correct intensities, signals for all ring proton environments and 18:9 intensity signals for two types of ^{t}Bu groups in the chemical shift range -2 to 67 ppm. ^{1}H NMR of **3b** in the same solvent shows a very similar pattern with exception of an additional set of three Ph group signals in 2:2:1 ratio and the absence of an intensity 9H signal.

Single crystals of [Li(THF)$_2$(PNN^{tBu})]CoCl$_2$ were grown by slow diffusion of pentane vapors into a concentrated THF solution at -45°C and analyzed with X-ray diffraction (Figure 4). The metal coordination sphere is similar to the parent compound (PNNH)CoCl$_2$ with τ_5 = 0.39 showing geometry closer to square pyramidal. Both metals occupy the plane of the aromatic rings of the ligand. The phosphorus lies out of this plane and has inequivalent ^{t}BuP groups with no signs of agostic interactions with Co1. The distance Co1-N2 is significantly shorter (by 0.044 Å) and the distance Co1-Cl2 is longer (by 0.064 Å) than in (PNNH)CoCl$_2$. Lithium is coordinated to pyrazolyl nitrogen N1, to Cl2 and to two THF molecules, together forming distorted tetrahedral geometry around the alkali metal. The main distortion from tetrahedral Li$^+$ is caused by steric clash between pyrazolyl ^{t}Bu and one of the coordinated THF. Overall, this shows that the first product in Scheme 1a is oversimplified and dehydrohalogenation is not the result. Instead a "proton to lithium metathesis" occurs and LiCl is retained, to satisfy both Lewis acid (Co) and Lewis basic (pyrazolyl β-nitrogen) sites.

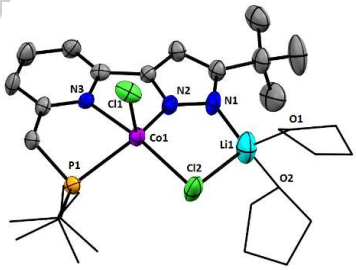

Figure 4. Mercury view (50% probabilities) of the nonhydrogen atoms of (Li(THF)$_2$(PNN^{tBu}))CoCl$_2$ **3a**, showing selected atom labelling; unlabeled atoms are carbon. Selected structural parameters: Co1-N2 2.034; Co1-N3 2.163; Co1-P1 2.466; Co1-Cl1 2.301; Co1-Cl2 2.363; Li1-Cl2 2.367; Li1-N1 1.678. Two THF molecules coordinated with Li1 and ^{t}Bu groups on phosphorous atom are shown in wireframe, for clarity.

The molecule (LiPNN)CoCl$_2$ can be presented in two resonance structures (Scheme 5) depending on which pyrazole ring nitrogen is considered as amidic. Chlorine Cl2 is equidistant from the two metals (Co1-Cl2 2.363; Li1-Cl2 2.367).

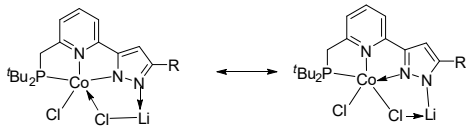

Scheme 5. Two resonance forms of (LiPNN)CoCl$_2$, as pyrazolate bridges Co^{II} and Li$^+$.

10.1002/chem.201700859

Deprotonation could also be performed with KHMDS and NaHMDS, with formation of the K and Na analogs than show lower solubility in THF but no difference in NMR spectra compared to Li analogs. Deprotonation of (PNN^{Ph}H)CoCl$_2$ **2b** with LiHMDS was performed under the same conditions, and the product showed spectroscopic data in agreement with the proposed structure (Fig. S14).

Redox Chemistry of 2 and 3.

A goal of multielectron catalysis stimulated brief study of the electrochemical behavior of both **2a** and **3a**. Cyclic voltammetry of (PNN^{tBu}H)CoCl$_2$ **2a** showed (Fig. 5) one quasireversible oxidation at 0.55 V associated with Co^{2+}/Co^{3+} and two irreversible 1ē reductions at -1.99 and -2.81 V vs. Fc/Fc$^+$. CV of complex **3a** was measured in 0.1 M TBAPF$_6$ electrolyte containing 0.5 M of LiCl to resolve reduction peaks and showed *quasireversible* oxidation and irreversible reduction waves. The oxidation peak is shifted by 0.35 V to more positive potential, in agreement with weakened donation from μ-Cl$^-$. Reduction of **3a** occurs at almost 0.5 V less negative potentials than for **2a** which made compound **3** our candidate for chemical reduction.

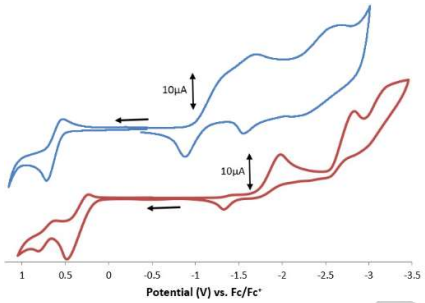

Figure 5. CV (1.5 to -3.2 V) of (PNN^{tBu}H)CoCl$_2$ **2a** (bottom) in THF/ 0.1 M [NBu$_4$]PF$_6$ at 100 mV/s. and [Li(THF)$_2$PNN^{tBu}]CoCl$_2$ **3a** (top) in THF/ 0.1 M [NBu$_4$]PF$_6$, 0.5 M LiCl at 100 mV/s. (CV without LiCl addition: see Fig. S60)

We used CO as a surrogate substrate for Co(I) here and as a spectroscopic probe to evaluate donor properties of different new ligands in their Co(I) complexes. Addition of 1 eq. of KC$_8$ to [Li(THF)$_2$PNN]CoCl$_2$ **3a** in THF under 1 atm of CO results in immediate color change from blue to red. After stirring for an additional 4 h at r.t., vacuum removal of unreacted CO caused immediate color change from *red* to *green*. Filtration from graphite and removal of the solvent yields green glassy solid. ^{1}H NMR of the green solid shows signals in a range 1 – 8 ppm, indicating diamagnetism and no evidence of paramagnetic species from -200 to 200 ppm; ^{31}P NMR shows one broad singlet at 105 ppm and ^{13}C NMR showed a set of signals from PNN ligand but no signal from carbonyl carbon, probably because of broadening by quadrupolar ^{59}Co. Addition of 1 atm of CO to a green solution causes immediate color change back to red and ^{31}P NMR shows a 15 ppm downfield shift of the singlet, all confirming the equilibrium in Scheme 6. ^{1}H NMR indicates minor changes in chemical shifts of PNN ligand protons and ^{13}C NMR shows a set of signals from PNN ligand and one broad signal from CO carbon at 203 ppm with no resolved coupling to phosphorus. We anticipated the green solid to be a square-planar Co(I) monocarbonyl, as typical for Co(I) complexes with monoanionic pincer ligands[12] and the red product to be dicarbonyl adduct (Scheme 6).

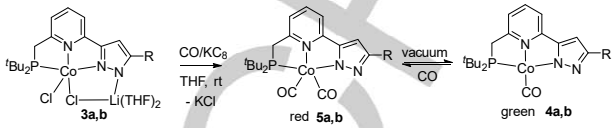

Scheme 6. Reduction of [Li(THF)$_2$PNN]CoCl$_2$ **3a** and **3b** under CO atmosphere.

Single crystal X-ray diffraction of the green monocarbonyl **4b** established (Figure 6) that it is (PNN^{Ph})Co(CO) and confirms four coordinate planar (τ_4 = 0.1) unsaturated Co(I) with no significant short *inter*molecular contacts involving the metal or the carbonyl. It also confirms the retention of two benzylic hydrogens, and the pyrazolate CNN angle, 106.4° confirms that this nitrogen is deprotonated; moreover, there is no evidence for hydrogen electron density near N in the final difference map. The Co-N distance to pyrazolate is shorter than that to pyridine, and the Co-C and C-O distances, 1.704 and 1.154 Å, respectively, reveal significant weakening of the CO bond. The phenyl ring has an angle of 29.8° to the pyrazolate ligand.

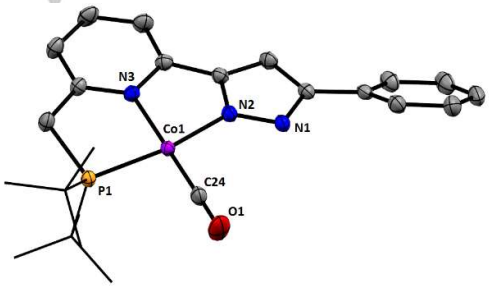

Figure 6. Mercury view (50% probabilities) of the nonhydrogen atoms of (PNN^{Ph})CoCO, showing selected atom labelling; unlabeled atoms are carbon. ^{t}Bu groups on phosphorous atom are shown without probability ellipsoids for clarity. Selected structural parameters: Co1-N2 1.899; Co1-N3 1.949; Co1-P1 2.156; Co1-C24 1.704; C24-O1 1.154; P1-Co1-N2 166.3; N3-Co1-C24 179.00; Co1-C24-O1, 178.76.

Surprisingly, IR spectra of freshly isolated **4a** or **4b** in THF each show *two* CO stretches, at 1885 and 1933 cm^{-1}, and always in different intensity ratio. When **4a** was stirred in Et$_2$O for 3 days, the stretch at 1885 disappears completely and formation of white precipitate was observed. When crystals of **4b** from the same batch that was analyzed by X-ray diffraction were dissolved in THF, only the 1933 cm^{-1} band was observed, consistent with the absence of LiCl. Altogether this suggests the reversible formation of a LiCl adduct, with equilibrium populations influenced by partial removal of LiCl during multiple solvent manipulations.

10.1002/chem.201700859

To test this hypothesis, an excess of solid LiCl was stirred with compound **4a** in THF and monitored by solution IR for 48h (Fig. 7).

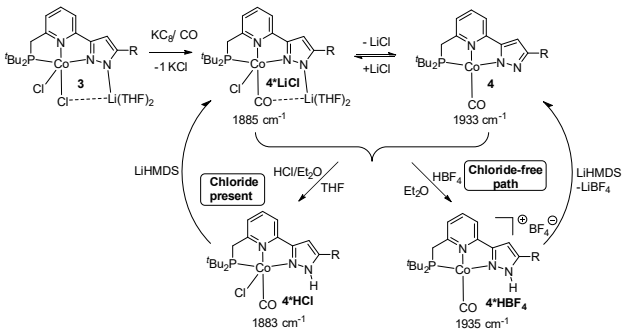

Scheme 7. Protonation and deprotonation of (PNN^{fBu})Co(CO) **4** with two different acids.

The band at 1933 cm^{-1} significantly decreases during reaction time and 1885 cm^{-1} stretch increases, in agreement with the equilibrium in Scheme 7 shifting to the right. When a THF solution of compound **4a** was mixed with preformed 0.5 M LiCl THF solution, IR detected the equilibrium established immediately and no changes of the spectra were observed after 12h. After addition of 1 atm of CO to a green solution of pure (LiCl-free) **4a** or **4b**, to form the red dicarbonyl, two IR bands at 1940 and 1994 cm^{-1} were observed, in agreement with the predicted structure. When LiCl adduct **4a·LiCl** was exposed to CO, three bands were observed at 1884, 1940 and 1994 cm^{-1}. This indicates that two species **5a** and **4a*LiCl** are present in solution and in fast equilibrium. The fact that the mixture of **4** with **4*LiCl** adduct or even together with **5** under CO atmosphere has only a single phosphorus NMR signal and also a single set of proton NMR signals shows that this equilibrium is rapid on the NMR timescale and is certainly rapid on the synthetic and laboratory timescales.

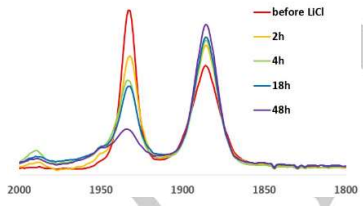

Figure 7. IR monitoring of reaction mixture of **4a** and LiCl in THF.

To further support the LiCl coordination hypothesis, a series of experiments (Scheme 7) were designed to create contrasting chloride-free and chloride-rich environments. Treatment of the mixture of **4a*LiCl** (nearly 1:1 ratio of 1885 and 1933 cm^{-1} bands) with HBF_4 yields a solution which contains a single carbonyl frequency, 1935 cm^{-1}. This species was then deprotonated with LiHMDS to form only a single carbonyl complex which has almost the same CO stretching frequency, but is due to pure **4**.

If the equilibrium mixture is instead treated with HCl·Et_2O, it converts to one monocarbonyl complex with frequency 1883 cm^{-1} (which rapidly precipitates) and this can be deprotonated with LiHDMS to give a species which shows primarily the 1885 cm^{-1} carbonyl frequency. This is best understood with the reactions in Scheme 7, where replacement of NH by NLi, with retention of chloride, leaves the CO stretching frequency nearly unchanged. All of this suggests that the two cobalt(I) monocarbonyl species are isomeric four coordinate Co(I) with free chloride counterion, and coordinated chloride in the five-coordinate saturated Co(I). Binding of chloride is apparently promoted in this case by the cationic charge of the four-coordinate cobalt complex, and certainly its lower CO frequency is consistent with better π basicity in the saturated cobalt, but it is interesting that the adduct formation constant is modest, able to be influenced by concentration and sample history. The ready loss of CO from (PNN)Co(CO)$_2$ **5** in Scheme 6 also shows the limited Lewis acidity of unsaturated Co(I) here. It is noteworthy that the CO frequencies of H and Li analogs are extremely similar. The low solubility of the protonated chloro complex (PNNH)CoCl(CO) **4a*HCl** is attributed to intermolecular hydrogen bonding between pyrazole H and chloride.

Cationic complex **4a*HBF$_4$** (Scheme 7) was isolated and characterized with IR, NMR and X-ray diffractometry. The IR of the product shows one stretch at 1935 cm^{-1} and ^{1}H NMR shows a set of signals for PNN^{fBu}H ligand including an acidic NH proton at 13 ppm (Scheme 8); one ^{31}P NMR singlet confirms formation of a single product. The identity of the NH proton was proven by ^{1}H/^{13}C HMBC NMR experiment, where the signal at 13 ppm in ^{1}H spectrum has a cross-peak with the ^{13}C NMR signals at 101.4, 154.6 and 159.7 ppm, that were independently assigned as pyrazole ring carbons. The carbonyl ^{13}C NMR signal appears at 201.8 ppm, and BF_4 appears in ^{19}F NMR as a singlet at -156.79 ppm. Single crystals of (PNN^{fBu}H)Co(CO)BF_4 were grown by slow diffusion of pentane vapors into a concentrated THF solution at -45ºC and analyzed with X-ray diffraction (Figure 8).

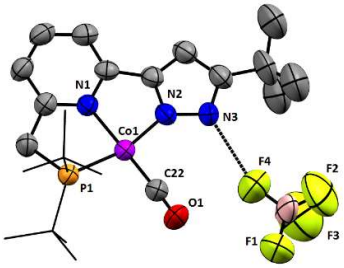

Figure 8. Mercury drawing (50%) of the nonhydrogen atoms of [(PNNH)Co(CO)]BF_4●THF **4a*HBF$_4$**, showing selected atom labelling. Unlabeled atoms are carbons, THF molecule is omitted, ^{t}Bu groups on phosphorous atom are shown without probability ellipsoids for clarity. Selected structural parameters: Co1-P1, 2.1738(19); Co1-N1, 1.954(5); Co1-N2, 1.939(5); Co1-C22, 1.731(7); O1-C22, 1.130(7); P1-Co1-N1, 84.32(15); P1-Co1-N2, 164.18(16); N1-Co1-N2, 80.5(2); P1-Co1-C22, 94.2(2); N1-Co1-C22, 178.3(3); N2-Co1-C22, 100.8(3).

10.1002/chem.201700859

Cobalt is square planar with τ_4 = 0.07. All metal heteroatom distances are shorter (Co-P by 0.306 Å, Co-N_{py} by 0.253 Å, and Co1-N_{pz} by 0.139 Å) compared to [PPNH]$CoCl_2$ **2a**, consistent with a low-spin state of Co(I). The phosphine has two equivalent ^{t}Bu groups with no signs of agostic interactions with Co1. The NH hydrogen forms a hydrogen bond with F4 of the counterion (N3•••F4 = 2.761 Å).

Cationic **4a*HBF$_4$** reversibly binds another CO molecule when exposed to 1 atm of CO (Scheme 8). The reaction mixture turns from deep green to red in the same manner as for [PNN^{tBu}]Co(CO) **4a** and IR showed two new bands at 1944 and 2007 cm^{-1} . Removal of CO atmosphere reverses the process. ^{1}H NMR of the CO adduct showed significant broadness of all peak corresponding to compound **5a*HBF$_4$** (but no broadness of solvent residual peaks) indicating that CO binding rate is closer to NMR timescale than in case of neutral **4a**.

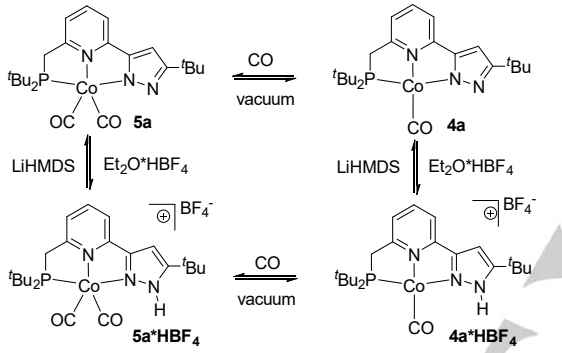

Scheme 8. Protonation and deprotonation of mono and dicarbonyl Co(I) adducts.

The ^{1}H and ^{31}P NMR spectra show broad peaks shifted upfield compared to the parent monocarbonyl, attributed to equilibrium between mono and dicarbonyl species. Treatment of both mono and dicarbonyl complexes with 1 eq. of LiHMDS (Scheme 8) removes HBF_4 with formation of neutral [PNN^{tBu}]Co(CO) **4a** and [PNN^{tBu}]$Co(CO)_2$ **5a**, respectively; with no signs of $LiBF_4$ retention, protonation is thus fully reversible. The absence of ^{19}F NMR signals in the isolated product after deprotonation indicates that $LiBF_4$ has been removed completely.

Benzylic Deprotonation.

Methylene protons on the phosphine arm are known to be acidic because of resonance stabilization of conjugate base by the pyridyl nitrogen. After treatment of **4a** or **4b** with 1 eq. of KHMDS in Et_2O or THF at r.t., a color change from green to violet was observed and ^{31}P NMR indicates consuming of starting material and formation of a single product (singlet at 99.2 ppm for **6a** Scheme 9). ^{1}H NMR shows a singlet with intensity of ^{1}H at 2.96 ppm indicating removal of one methylene proton (we designate this CH_2-deprotonated *dianionic* ligand as PNN^{R*}) accompanied by significant downfield shift of pyridyl protons associated with loss of aromaticity. ^{13}C NMR and ^{1}H/^{13}C HMBC and HMQC confirms the structure proposed for [Li(THF)$_2$PNN^{R*}]Co(CO). IR in Et_2O shows one band at 1851 cm^{-1}, a significant red shift, in agreement with pyridine nitrogen (trans to carbonyl) now being amidic compared to imine in previous examples: push/pull interaction increases back donation to CO.

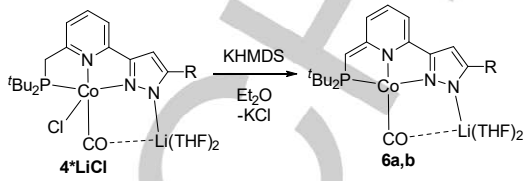

Scheme 9. Dearomatization of PNN ligand in its Co(I) carbonyl complex.

Single crystal X-ray diffraction study of **6a** (Fig. 9) confirmed what was established by spectroscopy but with the surprise that the alkali metal is lithium (not K from the KHMDS), and the lithium binds to pyrazolate nitrogen (2.005 Å), but also to carbonyl oxygen (2.394 Å) and to two THF molecules (1.922; 1.916 Å). There are no other short packing contacts with the carbonyl oxygen. The coordination geometry around cobalt(I) is planar, and only the lithium lies slightly out of that plane. The pattern of CC and CN distances (Fig. 10) confirms that the benzylic hydrogen has been removed by $N(SiMe_3)_2^{-1}$, and that pyridine aromaticity has been interrupted. The resulting amide nitrogen π lone pair can only interact constructively with a dπ orbital by a push/pull interaction involving one CO π^* orbital with the two occupied Co and amide π orbitals. The Co-C distance is indeed 0.021 Å shorter than in [PNN^{Ph}]Co(CO) **4b** and 0.048 Å shorter than in [(PNN^{tBu}H)Co(CO]BF_4 **4a*HBF$_4$** and the Co-N(amide) distance is not particularly short. The CO distance is 0.017 Å longer in [Li(THF)$_2$PNN*]Co(CO) **6a** than in [PNN^{Ph}]Co(CO) **4b** and 0.041 Å longer than in **4a*HBF$_4$**, in agreement with a higher degree of back donation and consequently 84 cm^{-1} lower CO frequency. Lithium binds two THF molecules and pyrazolate N, allowing additional interactions between cobalt-bound substrate and Li$^+$.

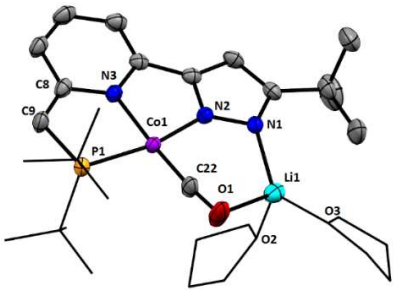

Figure 9. Mercury drawing (50%) of the nonhydrogen atoms of [Li(THF)$_2$P*NN^{tBu}Co(CO)] **6a**, showing selected atom labelling. Unlabeled atoms are carbons. ^{t}Bu groups on phosphorous atom and two coordinated THF molecules are shown without probability ellipsoids for clarity. Selected structural parameters: Co1-P1 2.185; Co1-N2 1.908; Co1-N3 1.926; Co1-C22 1.683; C22-O1 1.171; N1-Li1 2.005; Li1-O1 2.294; C8-C9 1.369; C8-N3 1.390; P1-Co1-N2, 166.0; N3-Co1-C22, 176.4; N2-Co1-C22, 96.2.

10.1002/chem.201700859

Collectively, these results show remarkable selectivity for retention of the Li^+ in competition with the larger alkali metal K^+. This may foretell a thermodynamic preference which could be used productively in future studies with this alkali metal/ligand transition metal partnership, enabled by pyrazolate.

Comparison of the bond lengths within the NNPCoCO unit of [Li(THF)$_2$PNN*^{tBu}]Co(CO) **6a** to those in [(PNN^{tBu}H)Co(CO)]BF$_4$●THF show the largest changes to be shortening of the CoC and lengthening of the CO distances on going from Li^+ to H^+ as electrophile on pyrazolate N.

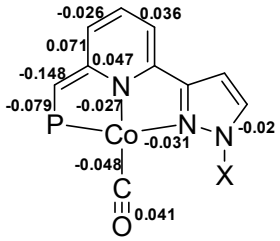

Figure 10. Significant differences (more than 0.020 Å) of bond lengths of [Li(THF)$_2$PNN^{tBu}*]Co(CO) **6a** and ([PNN^{tBu}H]Co(CO)BF$_4$ **4a*HBF$_4$**. Numbers obtained by subtraction of bond lengths in Å of **4a*HBF$_4$** from corresponding bond length in **6a**.Lewis structure is from the benzylic deprotonated PNN* form, showing bond length alternation after dearomatization.

Proton transfer Reactivity: Identifying basic sites.

Treatment of [Li(THF)$_2$PNN^{tBu}*]Co(CO) **6a** with H_2O in Et_2O or THF results (Scheme 10) in immediate color change from violet to green and IR indicates one stretch at 1935 cm^{-1} corresponding to [PNN]Co(CO) **4a**. The selectivity of this proton transfer was established by the analogous addition of D_2O, which initially shows half intensity CHD signal, but subsequent disappearance of methylene proton due to slower multiple H/D exchange (Fig. S57-58)

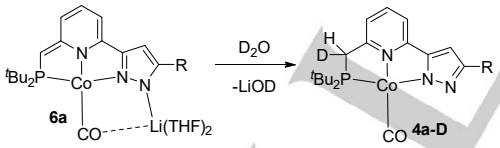

Scheme 10. Reaction of [Li(THF)$_2$PNN*]Co(CO) with D_2O/H_2O.

X-ray photoelectron spectroscopy (XPS): elemental composition and oxidation states

XPS measures the energy and intensity of core electrons of selected elements ejected by monochromatic X-rays. Intensity of ejected photoelectrons allow quantitation of each element, in terms of atom ratios, and binding energy, BE (ionization potential), is related to the electron richness, hence oxidation state of the element involved: higher BE correlates with higher oxidation state, hence more positive local charge at that element[13]. XPS was recently applied for better understanding of ligand-noninnocent behavior in pincer complexes of iron[14]. In the present case, we are interested in detecting the presence or absence of LiCl in **4** and **4*LiCl**; we measured XPS of two samples, one a homogenous mixture of **4a** and **4a*LiCl** (based on solution IR) and one a crystalline sample of pure **4b**. To facilitate analysis of BE, compounds **2a** and **3a** were also analyzed. Spectra of **4b** showed both Cl and Li are nearly absent, consistent with molecular structure data. For **4a*LiCl**, the measured Co/Cl ratio was almost 2:1 (see table 1) that agrees with 1:1 mole ratio in the mixture of **4a:4a*LiCl**. The measured Co/Li ratio is almost 4:1 but much lower sensitivity of XPS to Li atoms compared to Cl makes this number less reliable than the Co/Cl ratio, and the presence of Li in the sample was confirmed. Potassium is below detection limit on this sample, confirming that the reducing agent is not incorporated in this sample in the reduction process. For all samples, the measured Co to Cl, P, and N atomic ratios confirmed the proposed formulas (see Table 1).

Table 1. Atomic ratios in % measured (*calculated*) for cobalt complexes **2a**, **3a**, **4a*LiCl** and **4b**

	Co/P (*50:50*)	Co/N (*25/75*)	Co/Cl	Co/Li
2a	52/48	26/74	36/63 (*33/67*)	
3a	55/45	26/74	30/70 (*33/67*)	47/52 (*50/50*)
4a*LiCl	52/48	28/72	66/34	80/20
4b	52/48	27/73	93/7 (*100/0*)	91/9 (*100/0*)

In addition (Table 2), cobalt binding energies for compound **2a** and **3a** are in the range known for Co(II) complexes[15] and accompanied by shake-up peaks characteristic of Co(II). Binding energies of monovalent cobalt are expected to be ~1 eV lower than for Co(II). We obtained Co(I) BE by deconvolution of broad spectra (see SI for details) and Co2p$_{3/2}$ BE of **4a** and **4b** agrees with this prediction. Interestingly, the N1s BE of **2a** appears as two peaks in 2:1 ratio, assigned as NH pyrazolic nitrogen having higher BE. After deprotonation, N1s peak of **3a** shifts to lower BE (~0.3 eV), in agreement with ligand negative charge. Compound **3a** contains two inequivalent Cl atoms according to crystallographic data; they cannot be resolved in XPS but both Cl2p components are significantly (~0.7 eV) shifted to higher BE compared to **2a**. Presumably two THF molecules coordinated to Li were lost in the XPS instrument high vacuum, resulting in a polymeric structure with bridging lithium coordinated to several Cl atoms. Vacuum dried **3a** is almost insoluble in non-coordinating solvents; NMR spectra in CD_2Cl_2 following vacuum treatment showed evidence of aggregation (multiple species) and the absence of THF signals in the diamagnetic region, but after removal of CD_2Cl_2 and redissolving in THF, a single species was detected, supporting the occurrence of THF loss in UHV.

Table 2. Binding energies for cobalt complexes **2a**, **3a**, **4a*LiCl** and **4b** (see Fig. S61-64 for details).

	Co2p$_{3/2}$ eV	N1s eV	P2p eV	Cl2p$_{3/2}$; Cl2p$_{1/2}$ eV	O1s eV
2a	780.31	399.49+400.96 in 2:1 ratio	130.87	197.87; 199.35	

10.1002/chem.201700859

3a	780.20	399.19	130.77	198.54; 200.22	
4a*LiCl	779.31	399.05	130.72	197.89. 199.44	531.6
4b	779.44	399.16	130.75		531.9

Conclusions

Dehydrohalogenation of alkyl halides is the reaction which leads to olefins, hence unsaturation, and this is the logical link to use of the term unsaturation in metal complex chemistry, where $IrHCl_2(CO)(PR_3)_2$ was treated with base to give the 16 valence electron, hence "unsaturated," Vaska complex, $IrCl(CO)(PR_3)_2$.[16] When base is reacted with a metal ligand complex which contains an acidic proton on a ligand, then net removal of H and Cl yields a metal complex of unchanged oxidation state, but unsaturated at metal, due to removal of halide. This envisioned product is of special interest since the unsaturation at M is accompanied by Lewis basicity *at ligand*. If that lone pair is remote from M, then dehydrohalogenation has created a metal complex which is simultaneously a Lewis acid, at M, and a Lewis base, via the conjugate base lone pair (Scheme 1a). This is an attractive bifunctional species, but hinges on whether the chloride will actually be removed from the metal, or will be retained, in order to avoid Lewis acidity.

The acidity of the benzylic hydrogens here is exceptional because metal-coordinated P and pyridine are both electron withdrawing substituents on CH_2. In particular, coordinated phosphines should be compared to phosphonium substituents (P^V), hence highly stabilizing towards the conjugate base carbanion, allowing considerable precedent. *Both* benzylic arms have been singly deprotonated on a PNP pincer complex of Ni(II), where the buildup of negative charge on the dianionic ligand was determined, yet the CO_2 electrophile attacked benzylic carbon, with no bond formation between CO_2 and nickel[7e]. The singly benzyl deprotonated product failed to react with CO_2. In contrast, a singly deprotonated benzylic arm example on Re(I) augments this analogous CC bond formation with a Re/O bond[7d]. Other examples of pincer benzylic deprotonation have shown that Li^+ associates closely with the π system of the dearomatized *ring* of the conjugate base[7a-c].

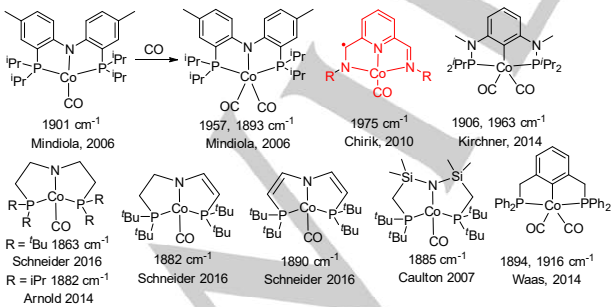

Figure 11. Cobalt(I) mono- and dicarbonyl complexes with monoanionic pincer ligand[12b-g, 17].

Several cobalt pincer complexes with monoanionic pincer ligands were reported in the last decade (Fig. 11)[12b-g, 17]. All of them contain amidic nitrogen trans to carbonyl, resulting in relatively low carbonyl bands 1863-1901 cm^{-1}. When neutral pyridine nitrogen is trans to CO as in Chirik's (PDI)Co(CO), almost 100 cm^{-1} higher stretch was observed. In our case in monoanionic PNN^{1-} the negatively charged pyrazolyl α-N is cis to carbonyl and moderate 1933 cm^{-1} shift of CO stretch was observed but second deprotonation to PNN^{*2-} dramatically increases back donation from metal to carbonyl to 1856 cm^{-1}. This makes PNN ligand able to manage the degree of substrate-complex interaction by addition or removal of proton on the ligand.

This work also shows that Li^+ is not simply a proton equivalent (*cf.* study of the "methane analog" CLi_4) but has productive capability, and not merely involving aggregation to $(LiX)_n$[18]. The retention of LiCl described here can be rephrased by considering the LiCl as a temporary *placeholder ligand*, subject to replacement by any substrate which binds better than chloride of LiCl. Our lack of recognition of this in Scheme 1 apparently originates from the fact that four coordinate $PNNCo^{II}Cl$ and three coordinate $(PNN)Co^{I}$ are sufficiently unsaturated that they retain chloride nucleophile, and then Li^+ is retained for charge balance. The frequent *retention* of Li^+ raises the question of its selectivity vs. other alkali metal cations, specifically K^+ here. The preference for Li^+ vs. deprotonating base cation K^+ in the conversion to $[Li(THF)_2PNN^{tBu*}]Co(CO)$ **6a** is remarkable: potassium is both larger than Li^+ and demands a higher coordination number. But it is also surprising that (PNN)Co(CO)*LiCl retains LiCl, since this four coordinate planar species **4** seems an attractive alternative which might not be Lewis acidic towards LiCl. It remains to be seen whether pyrazolate-bound K^+ or Li^+ has greater transforming impact on substrate bound locally. CO here serves as a surrogate to future substrates, and reveals that an electrophile on pyrazolate N indeed interacts with ligands bound trans to pyridine N. Said differently, pyrazolate here demonstrates its high affinity for *bridging* two metals, including the present heterobimetallic Co/Li^+ pair, and this can be a productive feature to further interact with substrate bound to a neighboring transition metal (Fig. 12).

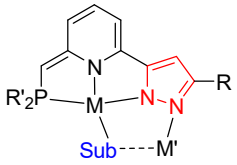

Figure 12. Pyrazolate as binding motif for bimetallic species.

The collective evidence from this work is that the general synthetic tool of dehydrohalogenation must confront the question of whether, when the base employed is an anion, its alkali metal cation will separate from the resulting conjugate base or bind to it. This is a question which always exists when deprotonating an acid HX with $M^+[Base^-]$: will the conjugate base X^- exist free, or only ion paired with M^+? In the present work, this is tied up with the fate of chloride on Lewis acid Co: will it remain coordinated, or depart

with the alkali metal? Clearly this option is eliminated if a neutral base is employed, and the resulting cationic protonated base is unreactive: P and sulfur ylides are examples of such bases.

Experimental Section

General. All manipulations were carried out under an atmosphere of ultra-high purity nitrogen using standard Schlenk techniques or in a glovebox under N_2. Solvents were purchased from commercial sources, purified using Innovative Technology SPS-400 PureSolv solvent system or by distilling from conventional drying agents and degassed by the freeze-pump-thaw method twice prior to use. Glassware was oven-dried at 150 °C overnight and flame dried prior to use. THF, including d_8-THF was stored over activated 4 Å molecular sieves or/and sodium metal pieces. NMR spectra were recorded in various deuterated solvents at 25 °C on a Varian Inova-400 or 500 spectrometers (^{1}H: 400.11 MHz, 500.11 MHz, respectively). Proton chemical shifts are reported in ppm versus solvent protic impurity, but referenced finally to $SiMe_4$. Mass spectrometry analyses were performed in an Agilent 6130 MSD (Agilent Technologies, Santa Clara, CA) quadrupole mass spectrometer equipped with a Multimode (ESI and APCI) source. All starting materials have been obtained from commercial sources and used as received without further purification. Cyclic voltammetry was done with Pt as the working electrode, Pt as the counter electrode, and Ag wire as the reference electrode. 0.1 M $TBAPF_6$ was employed as a supporting electrolyte, in THF solvent. In this medium, ferrocene has a peak-to-peak separation of 0.50 V. 1 mmol of each complex was dissolved in 10 mL of electrolyte solution. All CVs are referenced to internal Fc/Fc^+ as the standard, added at the end of a study of the experimental sample. Electrodes were polished when a new molecule was studied.

2-methyl-6-(5(3)-(*tert*-butyl)-1H-pyrazol-3(5)-yl)pyridine.

Sodium hydride (60 wt % in mineral oil, 0.612 g, 16 mmol) was added to a 250mL Schlenk flask and evacuated then refilled with N_2 3 times. This solid was suspended in 20 mL THF and stirred at RT for 10 min. Into this suspension was syringed in 1.70 mL (15 mmol) of 3,3-dimethylbutan-2-one over the course of 5 min. This mixture was allowed to stir at RT for 20 min and then heated to reflux, during which bubbling was observed and the mixture turned a dull yellow color. To this boiling mixture was added 1.89 g (12.5 mmol) of 2-methyl-6-methoxycarbonylpyridine dissolved in 12 mL THF. This addition was done over the course of 10 min and the mixture was then allowed to stir for an additional 4 h at reflux. The reaction mixture was cooled to RT and treated with 1.0 M aqueous HCl until the pH was between 6-7. This mixture was then extracted with 4 x 15 mL diethyl ether and washed with brine. The combined organic layer was dried over $MgSO_4$, filtered then solvent removed under vacuum to yield a yellow powder. This solid was then dissolved in 25 mL EtOH and brought to a boil. To this boiling solution was added 2 mL of $N_2H_4{\cdot}H_2O$ in 15 mL EtOH over the course of 10 min. This combined solution was refluxed for 2 hours with no additional color change. Solvent was removed under reduced pressure to leave a golden oil which was dissolved in 10 mL of THF and the solvent was removed again and the yellowish solid was formed. The solid was dissolved in a minimal amount of Et_2O and 5 fold excess of hexane was added. The white precipitate was collected by filtration after 48 h at -20°C. Colorless crystals (2.28 g, 85%). **^{1}H NMR** (400 MHz, $CDCl_3$ 298K): δ(ppm) 7.55 (t, $J_{H,H}$ = 7.5 Hz, 1H), 7.49 (d, $J_{H,H}$ = 7.5 Hz, 1H), 7.01 (d, $J_{H,H}$ = 7.5 Hz, 1H), 6.58 (s, 1H), 2.54 (s, 1H), 1.34 (s, 1H). **^{13}C NMR** (126 MHz, $CDCl_3$ 298K): δ(ppm) 158.17, 152.08, 136.80, 122.06, 116.81, 99.52, 31.68, 30.39, 24.50. **ESI-MS(+)** in THF: m/z = 216.2 $[M+H]^+$. **ESI-MS(-):** m/z = 214.2 $[M-H]^-$.

2-methyl-6-(5(3)-phenyl-1H-pyrazol-3(5)-yl)pyridine

Following the above procedure, using acetophenone instead of pinacolone, 2-methyl-6-(5-phenyl-1H-pyrazol-3-yl)pyridine was obtained as off-white solid in 75% yield. Spectroscopic data are in agreement with literature values[19]. **^{1}H NMR** (500 MHz, $CDCl_3$ 298K): δ(ppm) δ 7.85 (dd, $J_{H,H}$ = 7.7 Hz, 1Hz, 2H), 7.63 (t, $J_{H,H}$ = 7.7 Hz, 1H), 7.50 (d, $J_{H,H}$ = 7.7 Hz, 1H), 7.42 (t, $J_{H,H}$ = 8.3 Hz, 2H), 7.37 – 7.28 (m, 1H), 7.09 (d, $J_{H,H}$ = 7.2 Hz, 1H), 7.01 (s, 1H), 2.58 (s, 3H). **^{13}C NMR** (126 MHz, $CDCl_3$ 298K): δ(ppm) 152.57, 146.00, 141.81, 138.71, 131.28, 126.93, 122.85, 122.11, 119.82, 116.74, 111.17, 94.27, 18.58.

2-(5(3)-(*tert*-butyl)-1H-pyrazol-3(5)-yl)-6-((di-tert-butylphosphanyl)methyl)pyridine 1a

In glovebox in 25 ml scintillation vial 2.5 equivalents of nBuLi (2.5 M in hexane) were added dropwise to a solution of 2-methyl-6-pyrazolylpyridine (645 mg, 3 mmol) in THF (10 mL) at -78°C. The reaction mixture immediately changed its color to red-brown. The mixture was slowly warmed to room temperature during which formation of red precipitate was observed, stirred overnight and the red precipitate was formed. Then the solution was again cooled to -78°C and 1.2 equivalent of $ClP(^tBu)_2$ (550 mg, 3.1 mmol) was slowly added; after warming to room temperature stirring was continued for another 12 hrs. The reaction mixture was transferred to a Schenk flask containing a Teflon stirbar, 15 ml of Et_2O was added followed by degassed water (4 mL). The mixture was stirred for 15 min and then the organic layer was transferred by metal cannula and argon flow to an empty Schlenk flask. Evaporation of the solvent under reduced pressure gave almost pure product in ~75-85% yield (and 90% purity) as a yellowish oil. Purification of **1a** by recrystallization from Et_2O/pentane was performed and lead to significant loss of material due to a high solubility. Purity of crude material is enough for metallation and purification, if necessary, can be performed at the next stage. There are two pyrazole H-tautomers. **^{1}H NMR** (400 MHz, C_6D_6 298K): δ(ppm) *isomer 1* 11.55 (br.s; 1H, N*H*), 7.25 (d, $J_{H,H}$ = 7.7 Hz, 1H), 7.09 (t, $J_{H,H}$ = 7.7 Hz, 1H), 6.96 (d, $J_{H,H}$ = 7,7 Hz, 1H), 6.51 (s, 1H), 2.97 (d, $J_{H,P}$ = 9 Hz, 2H), 1.53 (s, 9H), 1.06 (d, $J_{H,P}$ = 11 Hz, 18H). *isomer 2* 10.70 (br.s; 1H, N*H*), 8.24 (m, 1H), 7.36 (m, 1H), 7.26 (m, 1H), 3.18 (bs, 2H), 1.12 (m, 27H). **^{31}P NMR** (162 MHz, C_6D_6 298K): δ(ppm) *isomer 1* 34.31; *isomer* 2 35.59. **^{13}C NMR** (100 MHz, C_6D_6 298K): δ(ppm) *isomer 1* + *isomer 2* 163.46, 162.63, 162.48, 153.77, 153.41, 147.81, 142.34, 136.67, 128.29, 128.17, 128.05, 127.93, 127.81, 123.05, 122.95, 116.64, 100.84, 99.68, 32.60, 32.31, 31.81, 31.04, 29.91, 29.77.

2-(5(3)-(phenyl)-1H-pyrazol-3(5)-yl)-6-((di-*tert*-butylphosphanyl)methyl)pyridine 1b.

Following the above procedure, compound **1b** was obtained in 75-85% yield and 90% purity. Recrystallization from THF/pentane was performed and lead to significant loss of material due to a high solubility. Purity of crude material is enough for metallation and purification, if necessary, can be performed at the next stage. Single tautomer: **^{1}H NMR** (400 MHz, CD_2Cl_2 298K): δ(ppm) δ 7.86 (d, $J_{H,H}$ = 7.9 Hz, 2H), 7.67 (t, $J_{H,H}$ = 7.9 Hz, 1H), 7.50 (d, $J_{H,H}$ = 7.6 Hz, 1H), 7.44 (t, $J_{H,H}$ = 7.6 Hz, 2H), 7.36 (d, $J_{H,H}$ = 7.6 Hz, 1H), 7.03 (s, 1H), 3.10 (d, $J_{H,P}$ = 3.3 Hz, 2H), 1.17 (d, $J_{H,P}$ = 11.2 Hz, 18H). **^{31}P NMR** (162 MHz, CD_2Cl_2 298K): δ(ppm) 37.25. **^{13}C NMR** (126 MHz, CD_2Cl_2, 298K) δ 162.48 (d, $J_{C,P}$ = 14.0 Hz), 136.92 (s), 128.62 (s), 127.81 (s), 125.46 (s), 123.29 (d, $J_{C,P}$ = 8.5 Hz), 116.43 (s), 99.49 (s), 31.85 (d, $J_{C,P}$ = 23.5 Hz), 31.66 (d, $J_{C,P}$ = 20.5 Hz), 29.46 (d, $J_{C,P}$ = 13.6 Hz).

[PNN^{tBu}H]CoCl$_2$ 2a

A solution of 359 mg (1 mmol) of **1a** in 10 mL of THF was added to the 130 mg (1 mmol) of $CoCl_2$. After stirring for 12 h at r.t, the reaction mixture became homogenous and turns to deep violet. The solution was concentrated to 2 mL under vacuum and 15 mL of Et_2O was added. The reaction mixture was placed at -45ºC overnight and violet solid precipitates from the solution. The mother liquor was decanted, the residue washed 1-2 times with 10 mL of Et_2O and dried under vacuum. Yield: 460 mg (96%) of violet microcrystalline powder. Additional recrystallization from THF/Et_2O can be performed for purification if necessary. Crystals suitable for X-ray diffractometry were grown by slow diffusion of pentane vapors into a concentrated THF solution at -35ºC. **^{1}H NMR** (400 MHz, CD_2Cl_2 298K): δ(ppm) 73.27 (br.s, 1H), 61.25 (s,1H), 59.01 (s, 1H), 57.00 (br.s, 2H), 47.96 (s, 1H), 22.20 (s, 1H), 3.26 (s, 9H), -1.82 (br.s, 18H). **ESI-MS(+)**: m/z = 453.15 [M-Cl]$^+$; **APCI-MS(+)**: m/z = 453.15 [M-Cl]$^+$; **XPS (BE eV):** Co2p$_{3/2}$ 780.31; Cl2p 197.87; N1s 399.45; 400.91; P2p 130.87

[PNN^{Ph}H]CoCl$_2$ 2b

Following the above procedure, compound **2b** was obtained in 90% yield as magenta powder. Solubility of **2b** in THF is lower than for **2a**; additional recrystallization could be performed from DCM/Et_2O if necessary. **^{1}H NMR** (400 MHz, CD_2Cl_2 298K): δ(ppm) 68.35 (s, 1H), 63.21 (s,1H), 58.63 (s, 1H), 54.63 (s,2H), 49.89 (s, 1H), 22.55 (s, 1H), 9.12 (s, 2H), 6.77 (s, 2H), 5.49 (s, 1H), -1.42(s, 18H). **ESI-MS(+)**: m/z = 473.12 [M-Cl]$^+$; **APCI-MS(+)**: m/z = 473.12 [M-Cl]$^+$

[Li(THF)$_2$PNN^{tBu}]CoCl$_2$ 3a

A suspension of 100 mg (0.2 mmol) of **2a** in 5 mL of THF was cooled to -78ºC and 2 mL of the precooled solution of LiHMDS (1.1 eq, 37 mg, 2.1 mmol) in 2mL of THF was added dropwise. The reaction mixture was stirred for 3 h at -78ºC and then slowly warmed to r.t. during which the color changed from violet to blue. The solvent was removed under vacuum, the residue was washed with Et_2O until the washings remain colorless, redissoved in THF, filtered through Celite, concentrated to 1 mL and addition of 5 mL of Et_2O caused precipitation of blue powder that was dried under vacuum. Yield: 80%. Single crystals suitable for X-ray diffractometry were grown by slow diffusion of pentane vapors into a concentrated THF solution at -45ºC. **^{1}H NMR** (400 MHz, THFd$_8$ 298K): δ(ppm) 66.63 (br.s, 2H), 55.83 (s, 1H), 36.41 (s, 1H), 27.75 (s, 1H), 9.50 (s,1H), 8.93 (s, 9H), -1.84 (br.s, 18H). **ESI-MS(+)**: m/z = 905.2 [((PNN)CoCl)$_2$ + H]$^+$; 911.1 [((PNN)CoCl)$_2$ + Li]$^+$; 947.1 [((PNN)CoCl)$_2$ + LiCl + H]$^+$ **APCI-MS(-)**: m/z = 487.0 [(PNN)CoCl$_2$. **XPS** Co2p$_{3/2}$ 780.20 eV (FWHM 1.75eV, asymmetric, shake-up 786.18 eV); N1s 399.19 eV (FWHM 1.67 eV, symmetric), P2p (FWHM 1.8 eV, asymmetric, spin-orbit components are not resolved), Cl 2p$_{3/2}$ 198.54 eV (FWHM 1.77eV, symmetric) Cl 2p$_{1/2}$ 200.22 eV (FWHM 1.55eV, symmetric); Li1s 55.36eV (FWHM 1.21, symmetric); Potassium and sodium adducts were obtained using KHMDS and NaHMDS, respectively, instead of LiHMDS, both showing lower solubility in THF compared to Li one.

[Li(THF)$_2$PNN^{Ph}]CoCl$_2$ 3b

Following the above procedure compound **3b** was obtained in 85% yield as blue powder. **^{1}H NMR** (400 MHz, THFd$_8$, 298K): δ(ppm) 64.57 (s, 2H), 58.28 (s, 1H), 42.81 (s, 1H), 35.31 (s, 1H), 15.75 (s, 2H), 13.70 (s, 1H), 13.09 (s, 2H), 7.04 (s, 1H), 2.44 (s, 18H). **ESI-MS(+)**: m/z = 925.2 [((PNN)CoCl)$_2$ + H]$^+$; 931.1 [((PNN)CoCl)$_2$ + Li]$^+$; 967.1 [((PNN)CoCl)$_2$ + LiCl + H]$^+$ **APCI-MS(-)**: m/z = 507.0 [(PNN)CoCl$_2$]$^-$.

[PNN^{tBu}]Co(CO) 4a and [PNN^{tBu}]Co(CO)*LiCl 4a*LiCl.

A solution of 64 mg (0.1 mmol) of LiPNNCoCl$_2$ in 5 mL of THF was added to a 25 mL Schlenk flask and freeze-pump-thawed 3 times to remove N_2 and then charged with 1 atm of CO. The flask was transferred to a glovebox and 14 mg of KC_8 was quickly added and the stopcock was tightly closed. Reaction mixture immediately turns brown and, in 30 min, deep red. The suspension was stirred for 12 h at r.t. and then CO was removed by vacuum. When vacuum was applied, the red reaction mixture immediately turns green and green suspension was filtered through Celite to remove graphite. The volatiles were removed yielding a green oil; 10 mL of Et_2O was added and the mixture was stirred for 12-48 h. Most of the residue was dissolved except for small amount of white solid and this solution was filtered through Celite, concentrated and pentane was added causing precipitation of green amorphous solid. If IR indicates presence of a second band at 1884 cm^{-1} repeated extraction with Et_2O is necessary. Yield: 80%. **^{1}H NMR** (400 MHz, THF-d$_8$, 298K): δ(ppm) δ 7.52 (t, $J_{H,H}$ = 7.7 Hz, 1H), 7.15 (d, $J_{H,H}$ = 7.7 Hz, 1H), 7.01 (d, $J_{H,H}$ = 7.1 Hz, 1H), 6.24 (s, 1H), 3.63 (d, $J_{H,P}$ = 9.3 Hz, 2H), 1.32 (d, $J_{H,P}$ = 11.3 Hz, 18H), 1.25 (s, 18H). **^{31}P NMR** (162 MHz, THF-d$_8$, 298K) δ(ppm) 103.2.). **^{13}C NMR** (126 MHz, tol-d$_8$ 298K): δ(ppm) 164.99 (s), 161.23(s), 156.07(s), 151.99(s), 138.79(s), 116.87(s), 114.19(s), 98.56(s), 34.70 (d, $J_{C,P}$ = 16.2 Hz), 34.50 (d, $J_{C,P}$ = 19.3 Hz), 32.51, 31.31, 28.78 (d, $J_{C,P}$ = 2.4 Hz). **IR (cm^{-1}) 4a** 1927 (KBr); 1933 (THF); 1940 (Et_2O); **4a*LiCl** 1881 (KBr); 1885 (THF or Et_2O); **XPS (BE, eV) 4a*LiCl** Co2p$_{3/2}$ 779.31 eV (FWHM 1.76 eV); N1s 399.05 eV (FWHM 1.79 eV), P2p 130.72 eV (FWHM 1.80 eV); O1s 531.60 eV (FWHM 2.05 eV); Cl 2p$_{3/2}$ 197.89 eV (FWHM 1.51eV) Cl 2p$_{1/2}$ 199.44 eV (FWHM 1.60eV); Li1s 55.3 eV (weak).

[PNN^{Ph}]Co(CO) 4b and [PNN^{Ph}]Co(CO)*LiCl 4b*LiCl

Following the above procedure, compound **3b** was obtained in 75% yield as a green powder. Pure samples of **3b** without LiCl coordinated were obtained by slow crystallization using pentane diffusion into concentrated THF solution and crystals suitable for X-ray diffractometry as well as sample for XPS analysis were collected from this batch. **^{1}H NMR** (400 MHz, THF-*d*$_8$, 298K): δ(ppm) δ 7.76 (d, $J_{H,H}$ = 7.5 Hz, 2H), 7.50 (m, 1H), 7.14 (t, $J_{H,H}$ = 7.5 Hz, 2H), 7.07 (d, $J_{H,H}$ = 7.5 Hz, 1H), 7.69 (m, 2H), 7.76 (d, $J_{H,H}$ = 7.5 Hz, 2H), 6.58 (s, 1H), 3.57 (d, $J_{H,P}$= 8.8 Hz, 2H), 1.33 (d, $J_{H,P}$ = 13.3 Hz, 18H). **^{31}P NMR** (162 MHz, THF-d$_8$, 298K) δ(ppm) 105.44. **^{13}C NMR** (126 MHz, THF-d$_8$ 298K): δ(ppm) 162.50 (d, $J_{C,P}$= 8.5 Hz), 155.60 (s), 155.57 (s), 153.98 (s), 153.95 (s), 153.00 (s), 139.59 (s), 136.08 (s), 127.67 (s), 125.15 (s), 124.53 (s), 117.66 (d, $J_{C,P}$= 9.1 Hz), 114.21 (s), 98.42 (s), 34.68 (d, $J_{C,P}$= 18.12 Hz), 34.61 (d, $J_{C,P}$= 17.8 Hz), 28.57 (d, $J_{C,P}$= 4.0 Hz). **IR (cm^{-1})** 1935 (THF); **XPS (BE, eV)** Co2p$_{3/2}$ 779.44 eV (FWHM 1.80 eV, asymmetric); N1s 399.16 eV (FWHM 1.67 eV), P2p 130.75 eV (FWHM 1.86 eV), O1s 531.9 eV (FWHM 2.2 eV).

[PNN^{tBu}]Co(CO)$_2$ 5a. [PNN^{tBu}]Co(CO) **4a** (22 mg, 0.05 mmol) was dissolved in THF-*d*$_8$ and added to J. Young NMR tube; after 3 pump-thaw operations the tube was pressurized with 1 atm of CO and reaction mixture turned from green to red. The dicarbonyl adduct exists only under CO atmosphere and turns green immediately after CO removal. **^{1}H NMR** (400 MHz, THF-*d*$_8$, 298K): δ(ppm) 7.57 (t, $J_{H,H}$ = 7.6 Hz, 1H), 7.30 (d, $J_{H,H}$ = 7.3 Hz, 1H), 7.04 (d, $J_{H,H}$ = 7.1 Hz, 1H), 6.41 (s, 1H), 3.73 (d, $J_{H,H}$ = 9.6 Hz, 2H), 1.38 (d, $J_{H,P}$ = 12.7 Hz, 18H), 1.31 (s, 9H). **^{31}P NMR** (162 MHz, THF-*d*$_8$, 298K) δ(ppm) 114.2. **^{13}C NMR** (125 MHz, THF-*d*$_8$, 298K) δ(ppm): 200.14, 164.08 (bs), 159.35 (s), 152.85 (s), 149.22 (s), 135.38 (s), 114.94 (s), 97.68 (s), 36.00 (d, $J_{C,P}$ = 14.7 Hz), 35.37 (d, $J_{C,P}$ = 20.1 Hz), 32.10, 30.69, 28.52. **IR (cm^{-1})** 1944, 1996 (Et_2O); 1936, 1994 (THF.)

[PNN^{Ph}]Co(CO)$_2$ 5b

Following the above procedure, yields a red solution in THF. **^{1}H NMR** (400 MHz, THF-d_8, 298K): δ(ppm) 7.78 (d, $J_{H,H}$ = 8.0 Hz, 2H), 7.51 (t, $J_{H,H}$ = 7.5 Hz, 1H), 7.34 (d, $J_{H,H}$ = 7.5 Hz, 2H), 7.14 (t, $J_{H,H}$ = 8.0 Hz, 2H), 6.98 (m, 2H), 6.90 (s, 1H), 3.67 (d, $J_{H,P}$= 10.3 Hz, 2H), 1.27 (d, $J_{H,P}$ = 13.6 Hz, 18H). **^{31}P NMR** (162 MHz, THF-d$_8$, 298K) δ(ppm) 116.35. **^{13}C NMR** (126 MHz, THF-d$_8$ 298K): δ(ppm) 200.65 (bs), 160.21 (d, $J_{C,P}$= 4.6 Hz), 154.83 (d, $J_{C,P}$= 4.0 Hz), 152.88 (s), 151.62 (s), 137.19 (s), 136.24 (s), 128.46 (s), 125.83 (s), 125.28 (s), 116.48 (d, $J_{C,P}$= 4.0 Hz), 116.39, 99.68 (s), 37.14 (d, $J_{C,P}$= 17.2 Hz), 36.31 (d, $J_{C,P}$= 21.0 Hz), 29.33 (d, $J_{C,P}$= 3.0 Hz). **IR (cm^{-1})** 1937, 1995 (THF.).

([PNNH]Co(CO))BF$_4$ 4a*HBF$_4$

[PNN]Co(CO) **4a** (45 mg, 0.1 mmol) was dissolved in 5 mL of Et$_2$O and 1 eq. of Et$_2$O*HBF$_4$ (13.6 µL) in 1 ml of Et$_2$O was added dropwise. Immediate formation of green precipitate was observed. The liquid phase was decanted and the residue was washed with 2x1 mL of Et$_2$O and dried under vacuum. Yield quantitative. **^{1}H NMR** (500 MHz, THFd$_8$, 298K): δ(ppm) 12.99 (s, 1H), 8.07 (t, $J_{H,H}$ = 7.8 Hz, 1H), 7.93 (d, $J_{H,H}$ = 7.8 Hz, 1H), 7.90 (d, $J_{H,H}$ = 7.8 Hz, 1H), 6.99 (s,1H), 4.11 (d, $J_{H,P}$ = 9.9 Hz, 2H), 1.47 (d, $J_{H,P}$ = 17.7 Hz, 18H), 1.43 (s, 9H). **^{31}P NMR** (162 MHz, THFd$_8$, 298K) δ(ppm) 103.46. **^{19}F NMR (376 MHz, THF-d8, 298K)**: δ(ppm) 156.79. **^{13}C NMR** (125 MHz, THFd$_8$, 298K): δ(ppm) = 201.75, 164.85, 159.72, 154.58, 150.47, 142.00, 124.02, 123.96, 118.49, 101.42, 35.58 (d, $J_{C,P}$ = 20.2 Hz), 35.31 (d, $J_{C,P}$ = 21.3 Hz), 31.60, 29.10, 28.66, 26.67. **IR (cm^{-1})** 1935 (THF). **MS(APCI$^+$)** m/z = 446.18 ([PNN^{tBu}H]Co(CO))$^+$. **MS(ESI$^+$)** m/z = 446.18 ([PNN^{tBu}H]Co(CO))$^+$.

([PNNH]Co(CO)$_2$)BF$_4$ 5a*HBF$_4$

[[PNN^{tBu}**H**]Co(CO))BF$_4$ **4a** (24 mg, 0.05 mmol) was dissolved in THF-d_8 and added to a J. Young NMR tube; after 3 pump-thaw operations, the tube was filled with 1 atm of CO and the reaction mixture turned from green to red. The dicarbonyl adduct exists only under CO atmosphere and turns green immediately after CO removal. **^{1}H NMR** (500 MHz, THF-d$_8$, 298K): δ(ppm) 13.07 (bs, 1H), 8.02 (bs, 2H), 7.83 (bs, 1H), 7.10 (bs,1H), 4.16 (bs, 2H), 1.54 (s, 9H), 1.38, 1.35 (bs, 18H). **^{31}P NMR** (162 MHz, THF-d$_8$, 298K) δ(ppm) 122.55. **^{19}F NMR (376 MHz, THF-d$_8$, 298K)**: δ(ppm) 156.78. **IR (cm^{-1})** 1944, 2007 (THF.).

K[PNN^{tBu}*]Co(CO) 6a

[PNN^{tBu}]Co(CO) **4a*LiCl** (calculated based on pure **4a**, 45 mg, 0.1 mmol) was dissolved in 5 mL of Et$_2$O and 1.1 eq. of KMHDS (21 mg) in 1 ml of Et$_2$O was added dropwise. The reaction mixture immediately turned from green to deep violet. After stirring for 2 h, the solution was filtered through Celite, concentrated and pentane was added, causing precipitation of dark solid. The solution was stored at -45°C for 12 h and then decanted. Solid material was dried in vacuum. Yield: 40 mg of dark-violet solid. Single crystals suitable for X-ray diffractometry were grown by slow diffusion of pentane vapors into a precooled saturated solution of **6a** in 5:1 heptane/THF mixture at -18°C. Crystals are extremely air-sensitive and must be handled in inert atmosphere. **^{1}H NMR** (400 MHz, THFd$_8$, 298K): δ(ppm) 6.23 (t, $J_{H,H}$ = 7.6 Hz, 1H), 5.85 (s, 1H), 5.74 (d, $J_{H,H}$ = 7.7 Hz, 1H), 5.27 (d, $J_{H,H}$ = 7.7 Hz, 1H), 2.96 (s, 1H), 1.36 (d, $J_{H,P}$ = 13.3 Hz, 18H), 1.28 (s, 9H). **^{31}P NMR** (162 MHz, THFd$_8$, 298K) δ(ppm) 99.2. **^{13}C NMR** (126 MHz, THFd$_8$, 298K) δ(ppm): 206.88, 206.17, 169.08, 168.94, 162.23, 155.47, 151.89, 132.34, 110.34, 110.23, 94.35, 93.30, 58.56 (d, $J_{C,P}$ = 51.3 Hz), 35.63 (d, $J_{C,P}$ = 23.4 Hz), 35.56, 31.78, 30.95, 28.99. **IR (cm^{-1})** 1851 (Et$_2$O).

K[PNN^{Ph}*]Co(CO) 6b

Following the above procedure, compound **6b** was obtained in 75% yield as a violet powder. **^{1}H NMR** (400 MHz, THFd$_8$, 298K): δ(ppm) 7.58 (d, $J_{H,H}$ = 7.5 Hz, 2H), 7.22 (t, $J_{H,H}$ = 7.4 Hz, 2H), 7.06 (t, $J_{H,H}$ = 7.4 Hz, 1H), 6.33 (s, 1H), 6.26 (m, 1H), 5.78 (d, $J_{H,H}$ = 8.3 Hz, 1H), 5.41 (d, $J_{H,H}$ = 6.2 Hz, 1H), 2.96 (s, 1H), 1.32 (d, $J_{H,P}$ = 12.9 Hz, 18H). **^{31}P NMR** (162 MHz, THFd$_8$, 298K) δ(ppm) 101.48. **^{13}C NMR** (126 MHz, THFd$_8$, 298K) δ(ppm): 169.81 48 (d, $J_{C,P}$= 19.2 Hz), 157.68 (s), 154.17 (s), 151.57 (s), 137.28 (s), 132.87 (s), 128.79 (s) 126.16 (s), 125.81 (s), 111.68 (d, $J_{C,P}$= 20.5 Hz), 97.63 (s), 95.21 (s), 59.90 (d, $J_{C,P}$= 54.5 Hz), 36.71 (d, $J_{C,P}$= 23.4 Hz), 29.80 (d, $J_{C,P}$= 4.0 Hz). **IR (cm^{-1})** 1852 (Et$_2$O).

Acknowledgements

This work was supported by the Indiana University's Office of the Vice President for Research and the Office of the Vice Provost for Research through the Faculty Research Support Program and the National Science Foundation, Chemical Synthesis Program (SYN), by grant CHE-1362127. ChemMatCARS Sector 15 is principally supported by the National Science Foundation/Department of Energy under grant number NSF/CHE-1346572. Use of the Advanced Photon Source was supported by the U. S. Department of Energy, Office of Science, Office of Basic Energy Sciences, under Contract No. DE-AC02-06CH11357.

Keywords: PNN pincer complex • cobalt • proton-responsive ligand • single-molecule FLP • metal-ligand cooperativity

[1] J. G. Andino, S. Mazumder, K. Pal and K. G. Caulton, Angewandte Chemie International Edition 2013, 52, 4726-4732.

[2] S. Gambarotta, F. Arena, C. Floriani and P. F. Zanazzi, Journal of the American Chemical Society 1982, 104, 5082-5092.

[3] a) S. F. McWilliams and P. L. Holland, Accounts of Chemical Research 2015, 48, 2059-2065; b) G. P. Connor and P. L. Holland, Catalysis Today.

[4] B. J. Cook, C.-H. Chen, M. Pink, R. L. Lord and K. G. Caulton, Inorganica Chimica Acta 2016, 451, 82-91.

[5] M. T. Whited, Beilstein J Org Chem 2012, 8, 1554-1563.

[6] a) G. van Koten, D. Milstein and SpringerLink (Online service) in Organometallic Pincer Chemistry, Vol. Springer Berlin Heidelberg : Imprint: Springer,, Berlin, Heidelberg, 2013, p. 1 online resource; b) K. J. Szabo, Pincer and pincer-type complexes : applications in organic synthesis and catalysis, p. xv, 302 pages.

[7] a) M. Feller, E. Ben-Ari, Y. Diskin-Posner, R. Carmieli, L. Weiner and D. Milstein, Journal of the American Chemical Society 2015, 137, 4634-4637; b) M. Feller, U. Gellrich, A. Anaby, Y. Diskin-Posner and D. Milstein, Journal of the American Chemical Society 2016, 138, 6445-6454; c) E. Fogler, J. A. Garg, P. Hu, G. Leitus, L. J. W. Shimon and D. Milstein, Chemistry – A European Journal 2014, 20, 15727-15731; d) M. Vogt, A. Nerush, Y. Diskin-Posner, Y. Ben-David and D. Milstein, Chemical Science 2014, 5, 2043-2051; e) M. Vogt, O. Rivada-Wheelaghan, M. A. Iron, G. Leitus, Y. Diskin-Posner, L. J. W. Shimon, Y. Ben-David and D. Milstein, Organometallics 2013, 32, 300-308.

[8] a) J. R. Khusnutdinova and D. Milstein, Angewandte Chemie International Edition 2015, 54, 12236-12273; b) H. Grützmacher, Angewandte Chemie International Edition 2008, 47, 1814-1818.

[9] A. W. Addison, T. N. Rao, J. Reedijk, J. van Rijn and G. C. Verschoor, Journal of the Chemical Society, Dalton Transactions 1984, 1349-1356.

[10] T. Steiner, Angewandte Chemie International Edition 2002, 41, 48-76.

[11] W. C. M. Duivenvoorden, Y.-n. Liu, G. Schatte and H.-B. Kraatz, Inorganica Chimica Acta 2005, 358, 3183-3189.

[12] a) S. S. Rozenel, R. Padilla, C. Camp and J. Arnold, Chemical Communications 2014, 50, 2612-2614; b) A. C. Bowman, C. Milsmann, C. C. H. Atienza, E. Lobkovsky, K. Wieghardt and P. J. Chirik, Journal of the American Chemical Society 2010, 132, 1676-1684; c) A. R. Fout, F. Basuli, H. Fan, J. Tomaszewski, J. C. Huffman, M.-H. Baik and D. J. Mindiola, Angewandte Chemie International Edition 2006, 45, 3291-3295; d) P. O. Lagaditis, B. Schluschaß, S. Demeshko, C. Würtele and S. Schneider, Inorganic Chemistry 2016, 55, 4529-4536; e) M. J. Ingleson, M. Pink, H. Fan and K. G. Caulton, Inorganic Chemistry 2007, 46, 10321-10334; f) S. Murugesan, B. Stöger, M. D. Carvalho, L. P. Ferreira, E. Pittenauer, G. Allmaier, L. F. Veiros and K. Kirchner, Organometallics 2014, 33, 6132-6140; g) M. A. Kent, C. H. Woodall, M. F. Haddow, C. L. McMullin, P. G. Pringle and D. F. Wass, Organometallics 2014, 33, 5686-5692.

[13] S. Hüfner, Photoelectron spectroscopy : principles and applications, Springer, Berlin ; New York, 2003, p. xv, 662 p.

[14] B. Butschke, K. L. Fillman, T. Bendikov, L. J. W. Shimon, Y. Diskin-Posner, G. Leitus, S. I. Gorelsky, M. L. Neidig and D. Milstein, Inorganic Chemistry 2015, 54, 4909-4926.

[15] a) J. K. Kouba, J. L. Pierce and R. A. Walton, Journal of Organometallic Chemistry 1980, 202, C105-C107; b) C. A. Strydom and H. J. Strydom, Inorganica Chimica Acta 1989, 159, 191-195.

[16] L. Vaska and J. W. DiLuzio, Journal of the American Chemical Society 1962, 84, 679-680.

[17] M. L. Scheuermann, S. P. Semproni, I. Pappas and P. J. Chirik, Inorganic Chemistry 2014, 53, 9463-9465.

[18] a) E. D. Jemmis, J. Chandrasekhar, E. U. Wuerthwein, P. v. R. Schleyer, J. W. Chinn, F. J. Landro, R. J. Lagow, B. Luke and J. A. Pople, Journal of the American Chemical Society 1982, 104, 4275-4276; b) F. J. Landro, J. A. Gurak, J. Chinn, R. Newman and R. Lagow, Journal of the American Chemical Society 1982, 104, 7345-7346.

[19] A. Chadghan, J. Pons, A. Caubet, J. Casabó, J. Ros, A. Alvarez-Larena and J. Francesc Piniella, Polyhedron 2000, 19, 855-862.

10.1002/chem.201700859

WILEY-VCH

Entry for the Table of Contents (Please choose one layout)

Layout 1:

FULL PAPER

A pyridyl pincer ligand is introduced to incorporate five different functionalities via a P^{t}Bu$_2$ and pyrazole pincer ligand arms. Ligand properties in neutral mono- and dianionic form were investigated on Co(I) and (II) complexes. Concept of single-molecule frustrated Lewis pair (FLP) was discussed and alkaline metal chlorides was used as a model substrate to show FLP behavior.

((Insert TOC Graphic here: max. width: 5.5 cm; max. height: 5.0 cm))

*Author(s), Corresponding Author(s)**

Page No. – Page No.

Title

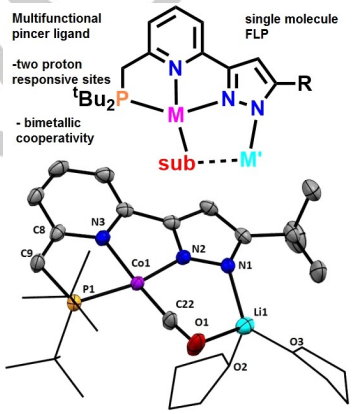

Layout 2:

FULL PAPER

((Insert TOC Graphic here; max. width: 11.5 cm; max. height: 2.5 cm))

*Author(s), Corresponding Author(s)**

Page No. – Page No.

Title

Text for Table of Contents